Struct Multidisc Optim (2013) 48:717–730
DOI 10.1007/s00158-013-0941-6

RESEARCH PAPER

On the similarities between micro/nano lithography and topology optimization projection methods

Miche Jansen · Boyan S. Lazarov · Mattias Schevenels · Ole Sigmund

Received: 13 December 2012 / Revised: 12 March 2013 / Accepted: 27 April 2013 / Published online: 12 June 2013

Abstract The aim of this paper is to incorporate a model for micro/nano lithography production processes in topology optimization. The production process turns out to provide a physical analogy for projection filters in topology optimization. Blueprints supplied by the designers cannot be directly used as inputs to lithographic processes due to the proximity effect which causes rounding of sharp corners and geometric interaction of closely spaced design elements. Therefore, topology optimization is applied as a tool for proximity effect correction. Furthermore, it is demonstrated that the robust projection filter can be used to account for uncertainties due to lithographic production processes which results in manufacturable blueprint designs and eliminates the need for subsequent corrections.

Keywords Topology optimization · Electron beam lithography · Proximity effects · Robust design · Projection filters · Design regularization

1 Introduction

Topology optimization (Bendsøe and Sigmund 2004) has become a popular tool for obtaining optimal designs in a broad range of problems varying from large mechanical assemblies and structures with a characteristic length of several hundred meters to photonic designs in nanoscale. Most of the applications reported in the literature are in the conceptual and the preliminary design stages and manual intervention is required later in order to obtain a complete manufacturable design. During the postprocessing phase the designer might severely affect the design performance and violate the design constraints. Therefore, modification of the original design and manual decision making steps are undesirable. Recently, the topology optimization method has been extended (Sigmund 2009; Wang et al. 2011b; Schevenels et al. 2011; Chen and Chen 2011; Jang et al. 2012) to include geometric imperfections in the design process. The modified optimization process results in manufacturable topologies by requiring lack of sensitivity of the design performance with respect to uncertainties in the geometry. The process removes the manual decision phase and the full design cycle is, for example, demonstrated in the design of directly manufacturable 3D material microstructures in Andreassen et al. (2012).

The imperfection models discussed above mimic the possible errors in the optimized topology, however, until now they have not been linked to any specific production process. As demonstrated in Lazarov et al. (2012) the model for the uncertainties may have significant influence on the optimized topology and, therefore, it is important to take into account the actual production technology in the optimization process. The focus in this article is on providing and demonstrating the link between the threshold projection schemes utilized in topology optimization and micro/nano-lithography production technology. The design discretization in the presented optimization formulations is based on actual physical quantities rather than on a pure mathematical discretization. The representation is applied for design

M. Jansen (✉)
Department of Civil Engineering, KU Leuven,
Kasteelpark Arenberg 40, 3001 Leuven, Belgium
e-mail: miche.jansen@bwk.kuleuven.be

B. S. Lazarov · O. Sigmund
Department of Mechanical Engineering, Solid Mechanics,
Technical University of Denmark, Nils Koppel's Allé,
Building 404, 2800 Lyngby, Denmark

M. Schevenels
Department of Architecture, Urbanism and Planning, KU Leuven,
Kasteelpark Arenberg 1, 3001 Leuven, Belgium

of dose and mask patterns in micro/nano-lithography. Optimizing the mask pattern cannot prevent the formation of small features in design, violating the design constraints and altering the design performance. Therefore, the production process is introduced in the optimization algorithm and by requiring robustness of the design performance the existence of length scale and manufacturability of the optimized design (Wang et al. 2011b) is confirmed again.

The remainder of this paper is organized as follows. In the following section, the reader is introduced to electron beam lithography (EBL) and the effects influencing the uncertainties in this production process. The link between topology optimization projection methods and EBL is discussed in detail in Section 3. The optimization algorithm is exemplified for the design of lithographic mask patterns in Section 4. Different input dose regularization strategies aiming at maximal contrast, minimal complexity, and minimal production time are elaborated in Section 5. Section 6 addresses the robustness of the lithographic pattern with respect to uncertainties in the EBL process. In Section 7, the optimal design of a compliant mechanism produced by means of EBL is considered. Finally, possible extensions to optical production processes are discussed in Section 8.

2 Electron beam lithography

Electron beam lithography (EBL) is often applied in small volume production of micro- and nano-structures etched out of a solid layer of material. The setup for electron beam lithography usually consists of two material layers. The substrate material, e.g. silicon, is covered by a polymeric electron-beam-sensitive resist. The goal of EBL is to write a pattern in the resist corresponding to the structure which is to be manufactured. This pattern is later transferred to the substrate by means of an etching procedure during which the resist serves as a protective layer for the substrate.

The two main phases of the EBL process are schematically summarized in Fig. 1. First, the resist is exposed at specified locations to electrons originating from an electron lithography system (Fig. 1a). Exposing the resist to the electrons energy causes local changes in the molecular weight of the polymeric material. A negative resist (e.g. HSQ) generates new bonds when exposed, while in an exposed positive resist such as PMMA chemical bonds are broken. After exposure, the resist is processed further in the development phase during which a solvent is added in order to dissolve and wash away molecules with a smaller molecular weight. As a results, positive resist is removed wherever it has been sufficiently exposed (Fig. 1b), while in a negative resist the exposed regions are retained on the substrate (Fig. 1c). This procedure enables the formation of specific patterns on micro- and nanoscale. The following sections present a mathematical model which is frequently applied in the literature to describe the EBL process.

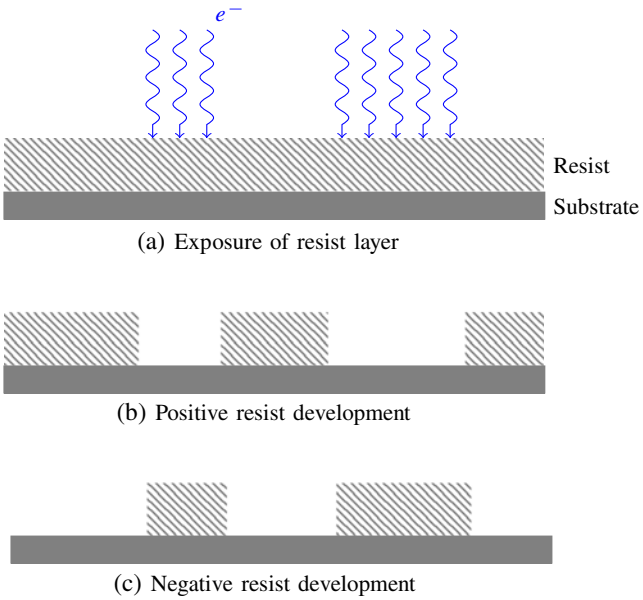

(a) Exposure of resist layer

(b) Positive resist development

(c) Negative resist development

Fig. 1 Electron beam lithography production process

2.1 Resist exposure

The technological aspects of the electron beam system and resist exposure are, for example, described in more detail by Suzuki (2007). Loosely speaking, an electron gun is used to emit an electron beam and a magnetic or electrostatic deflector directs the beam to the correct location on the resist. The total incident dose of electrons (i.e. the charge density per unit area) directed on the resist, is given by:

$$D(\mathbf{x}) = T(\mathbf{x})I \tag{1}$$

where the exposure time $T(\mathbf{x})$ represents the time the electron beam is pointed at location $\mathbf{x}$ and I is the beam current. Since the exposure time can be specified separately for every point, the dose $D(\mathbf{x})$ can vary in space and can, therefore, be modeled as a continuous variable. For this reason, EBL is a very flexible procedure compared to optical lithography which usually requires a mask to illuminate the correct shape on the resist. A drawback, however, is the relatively low throughput of EBL due to the high writing times resulting from the point-by-point exposure of the resist (McCord and Rooks 1997).

When an incident electron beam penetrates the resist, the solid material interacts with the electrons which causes the electrons to be deviated from their original path (e.g. Dobisz et al. 2007). The electron scattering events are often divided in a forward and a backward component (Fig. 2a). The forward scattering is attributed to interactions between

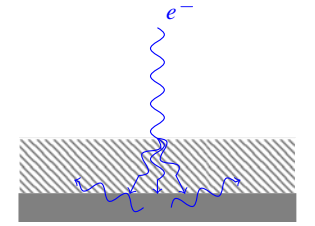

(a) Electron scattering

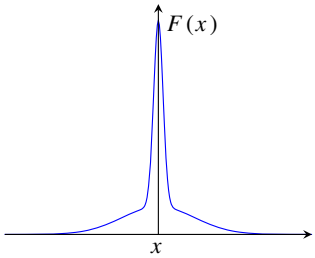

(b) Double Gaussian point spread function $F(x)$

Fig. 2 Forward and backward scattering of electrons and resulting energy distribution for a point source

the electrons and the molecules of the solid material layers which causes small angle in-elastic deflections of the electrons. If the target molecule is part of the resist, the molecular chain may change (i.e. resist being exposed) and a secondary electron may be generated. A portion of the electrons that reach the substrate layer, is reflected by the substrate molecules and elastically scattered at a large angle back into the resist layers at a significant distance from the incident beam. Due to these scattering events, the energy exposure of the resist by the e-beam is not perfectly localized. The energy leakage to the neighborhood of the e-beam is described by the point spread function (PSF) $F(\mathbf{x})$ which expresses the energy distribution of an incident point source due to scattering of electrons and the finite radius of the electron beam. The forward and backscattering component in electron beam lithography are often approximated in the PSF $F(\mathbf{x})$ as a sum of two Gaussians (e.g. Chang 1975):

$$F(\mathbf{x}) = \frac{1}{\pi(1+\tau)}\left(\frac{1}{\alpha_\mathrm{f}^2}\exp\left(-\frac{\|\mathbf{x}\|_2^2}{\alpha_\mathrm{f}^2}\right) + \frac{\tau}{\alpha_\mathrm{b}^2}\exp\left(-\frac{\|\mathbf{x}\|_2^2}{\alpha_\mathrm{b}^2}\right)\right) \tag{2}$$

where the backscatter ratio τ represents the fraction of backscattered electrons and α_f and α_b are the effective widths of the forward and backward scattered electron beams, respectively. Although the parameters α_f, α_b and τ are functions of a number of factors such as resist thickness and electron energy (Anderson et al. 2001), they are assumed to be constant for the specific setup applied during the exposure. Figure 2b illustrates the influence of forward and backscattering by showing a typical PSF with $\alpha_\mathrm{f} = 0.13\ \mu\mathrm{m}$, $\alpha_\mathrm{b} = 1\ \mu\mathrm{m}$ and $\tau = 1.15$ (Haslam and McDonald 1986)[1]. While the forward component mainly consists of electrons deflected at a small angle, the elastic backscattered electrons usually constitute a much broader spread of energy.

The energy exposure $E(\mathbf{x})$ of the resist corresponding to a given dose distribution $D(\mathbf{x})$ is determined by the convolution of the input dose $D(\mathbf{x})$ and the point spread function $F(\mathbf{x})$:

$$E(\mathbf{x}) = (F * D)(\mathbf{x}) = \int_{\mathbb{R}^2} F(\mathbf{x}-\mathbf{s})D(\mathbf{s})\mathrm{d}\mathbf{s} \tag{3}$$

2.2 Resist development

The development phase consists of a number of smaller steps in practice (McCord and Rooks 1997). Numerous resist development models with varying complexity are available (Dill et al. 1975; Madjarova 1992; Randall et al. 1999). The simplest model is the constant threshold model (Brunner and Ferguson 1996) where it is assumed that the process works as a perfect selector function between exposed and underexposed material. In a positive resist, material which has been exposed to a level above the clearing energy (Wüest et al. 2004), is removed, while the opposite occurs in a negative resist. The resulting patterns written in the positive and negative resist can be expressed as a function of the energy exposure:

$$P_+(\mathbf{x}) = H(E_\mathrm{cl} - E(\mathbf{x})) = \begin{cases} 1 & \text{if } E(\mathbf{x}) \le E_\mathrm{cl} \\ 0 & \text{if } E(\mathbf{x}) > E_\mathrm{cl} \end{cases} \tag{4}$$

$$P_-(\mathbf{x}) = H(E(\mathbf{x}) - E_\mathrm{cl}) = \begin{cases} 0 & \text{if } E(\mathbf{x}) < E_\mathrm{cl} \\ 1 & \text{if } E(\mathbf{x}) \ge E_\mathrm{cl} \end{cases} \tag{5}$$

where $P_+(\mathbf{x})$ and $P_-(\mathbf{x})$ are the patterns written in a positive and negative resist, respectively, E_cl is the clearing energy and $H(x)$ is the Heaviside step function.

2.3 Proximity effects

The energy leakage due to electron scattering causes interaction between the energy densities of nearby objects in a pattern. As a result, the geometries of objects in the

[1] These values are strongly dependent on the technology at hand. Values $\alpha_\mathrm{f} = 0.013\ \mu\mathrm{m}$, $\alpha_\mathrm{b} = 34\ \mu\mathrm{m}$ and $\tau = 0.512$ were reported for a ZEP520 resist material and a more modern EBL system. It can be expected that the backscattering component will approximately lead to a uniform increase of the background exposure for such large differences between α_f and α_b.

written pattern are influenced by the surrounding pattern distribution. This phenomenon is referred to as the proximity effect which is a well-known problem in electron beam lithography (e.g. Chang 1975; Haslam and McDonald 1986). The effects are not limited to electron beam lithography and can also occur in optical lithography where diffraction of light causes similar problems (e.g. Levinson and Arnold 1997).

Figures 3 and 4 illustrate the influence of proximity effects on a raster design with varying feature size and intermediate distances. The energy leakage, i.e. the smoothing effect introduced by the bandlimited e-beam system, reduces the correspondence between the geometry of the input dose (Fig. 3a) and the written pattern (Fig. 3c): sharp corners in the input dose become rounded in the written pattern, small objects may be underexposed and do not show in the pattern. Furthermore, the geometric errors are more severe for closely spaced objects: the energetic interference of the objects on the right side causes the intermediate gap to be closed in the written pattern.

When the input dose is chosen to resemble the shape of the desired output pattern, proximity effects ultimately cause a degradation of the pattern fidelity (i.e. correspondence between the fabricated and the desired pattern).

(a) Dose $D(\mathrm{x})$

(b) Exposure $E(\mathrm{x})$

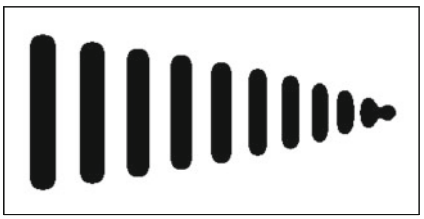

(c) Pattern $P(\mathrm{x})$

Fig. 3 Proximity effects

Fig. 4 Proximity effects - comparison between blueprint design (courtesy of F. Wang) obtained by topology optimization (Wang et al. 2011a) shown in *red*, and manufactured photonic crystal shown in *gray* (courtesy of Dr. Lars H. Frandsen)

Section 4 discusses proximity effect correction methods which adjust the input dose in order to compensate for the proximity effect and improve the pattern fidelity.

3 Lithography versus topology optimization

It can be seen that the lithographic manufacturing process is similar to Heaviside projection filtering in density based topology optimization (Guest et al. 2004; Sigmund 2007). In order to clarify this statement, we will first briefly recapitulate how density filters are employed in topology optimization. The design domain Ω in which the optimal design is sought, is discretized by means of n_e finite elements and the distribution of material in the domain is represented by assigning a constant material density $\bar{\rho}_e$ to every element. The densities are collected in the vector $\bar{\boldsymbol{\rho}} \in \mathbb{R}^{n_\mathrm{e}}$. The densities $\bar{\boldsymbol{\rho}}$ can vary continuously in the interval [0; 1] where 0 and 1 imply the absence or presence of material, respectively. The material properties relevant for the optimization problem are expressed as a function of the physical densities $\bar{\boldsymbol{\rho}}$ by means of the Solid Isotropic Material with Penalization (SIMP) interpolation (Bendsøe 1989; Zhou and Rozvany 1991). In a mechanical problem, for example, the interpolation of the Young's modulus is formulated as:

$$E_e = E_{\min} + (E_0 - E_{\min})\bar{\rho}_e^p \tag{6}$$

where E_0 and $E_{\min}$ are the Young's moduli of the material and void phase, respectively. The penalization parameter is typically chosen $p = 3$ in order to penalize intermediate densities and force the solution to a binary {0; 1} design.

A density filter is applied in order to eliminate checkerboard problems and mesh–dependency of the solution (Bourdin 2001; Bruns and Tortorelli 2001). In this case, a new set of independent (non-physical) design variables $\boldsymbol{\rho} \in \mathbb{R}^{n_\mathrm{e}}$ is introduced in the optimization problem. The design space is limited by filtering $\boldsymbol{\rho}$ with a smoothing kernel $\kappa(\mathbf{x})$:

$$\tilde{\rho}_e = (\boldsymbol{\kappa} * \boldsymbol{\rho})_e = \frac{\sum_{j=1}^{n_\mathrm{e}} \kappa(\mathbf{x}_e - \mathbf{x}_j) v_j \rho_j}{\sum_{j=1}^{n_\mathrm{e}} \kappa(\mathbf{x}_e - \mathbf{x}_j) v_j} \tag{7}$$

where v_j are the element volumes and x_e the location of the element centers. The kernel is typically a conic function $\kappa(\mathbf{x}) = \max(R - \|\mathbf{x}\|_2, 0)$ or a Gaussian function (Bruns and Tortorelli 2001). In order to remove the gray transition zones between material and void phase caused by the smoothing effect of the density filter, the intermediate variables $\tilde{\boldsymbol{\rho}}$ are projected by a regularized Heaviside function (Guest et al. 2004; Xu et al. 2010; Wang et al. 2011b):

$$\bar{\rho} = H_{\mathrm{c}}(\tilde{\rho}; \eta, \beta) = \frac{\tanh(\beta\eta) + \tanh(\beta(\tilde{\rho} - \eta))}{\tanh(\beta\eta) + \tanh(\beta(1 - \eta))} \tag{8}$$

where β is a steepness parameter and $\eta \in [0; 1]$ is the threshold value of the projection.

Figure 5 shows the similarity between the EBL model and projection filtering in topology optimization. The outline of this comparison shows that the EBL process and the resulting proximity effects can be incorporated into topology optimization by identifying the optimization variables $\boldsymbol{\rho}$ as the input dose $D(\mathbf{x})$ to the electron beam system. In this case, the density filter corresponds to the limited resolution of the lithography system which is modeled by the PSF $F(\mathbf{x})$. The intermediate densities $\tilde{\boldsymbol{\rho}}$ correspond to the resulting energy distribution $E(\mathbf{x})$ due to electron scattering (or diffraction in optical lithography) and the physical design

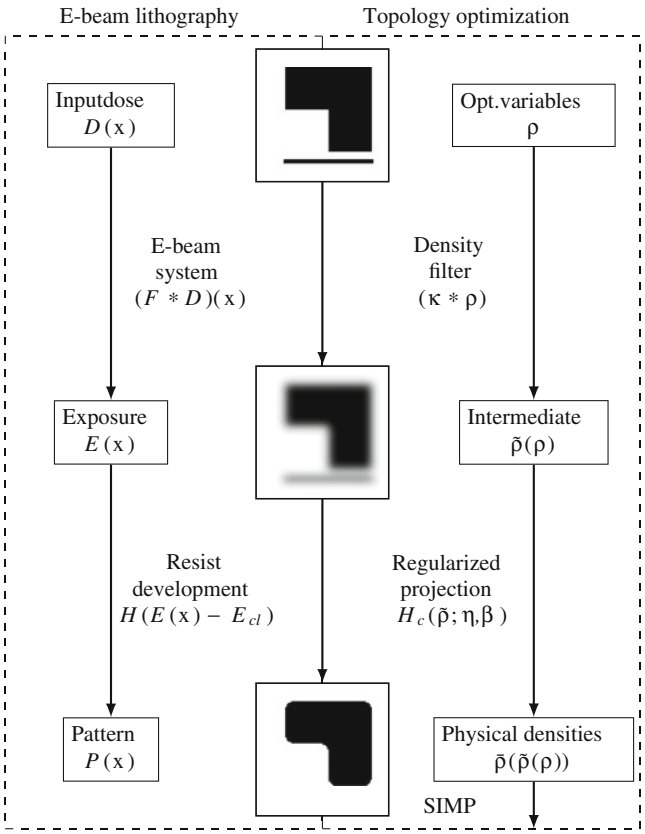

Fig. 5 Comparison of the electron beam lithography process and heaviside projection filtering in topology optimization

$\bar{\boldsymbol{\rho}}$ coincides with the written pattern $P(\mathbf{x})$ in electron beam lithography.

4 Proximity effect correction

In practice, the designer will provide the written pattern, i.e. the structure which he or she would like to manufacture, to the production unit. However, due to the occurrence of proximity effects, the desired pattern is often not directly usable as input to the lithography system. Instead, the input dose is modified by means of a proximity effect correction (PEC) method in order to improve the pattern fidelity, i.e. the correspondence between the fabricated and the desired pattern. Various approaches to PEC for electron beam and optical lithography have been developed for this purpose. Rule-based methods such as the PYRAMID algorithm (Lee et al. 1991) apply a constant dose for the complete pattern while the shape of objects are corrected based on predefined rule tables. Such an empirical approach has a relatively low computational cost, but is also characterized by a low flexibility and is often limited to standard integrated circuits (Dobisz et al. 2007). Owen and Rissman (1983) developed the GHOST method which is used to correct errors due to backscattered electrons in EBL.

Here, we consider proximity effect correction as the inverse problem of finding a suitable input dose for the desired output pattern (Peckerar et al. 1995, 2007). With the insights developed in the previous sections, we can apply topology optimization algorithms to solve this optimization problem. The numerical approaches to PEC in lithography (Harafuji et al. 1993; Peckerar et al. 1995; Poonawala and Milanfar 2007; Yu and Yu 2010; Jia and Lam 2011) employ a pixel based representation of the pattern similar to the finite element discretization in topology optimization. In the specific case of a linear representation of the lithography system, proximity effect correction can be formulated as a linear programming problem (Peckerar et al. 1995). In a more general setting, the inverse problem can be stated as a least-squares optimization problem:

$$\boldsymbol{\rho}^{\star} = \underset{\mathbf{0} \le \boldsymbol{\rho} \le \mathbf{1}}{\arg\min} \quad f_{\mathrm{pec}}(\boldsymbol{\rho}) = \frac{1}{n_{\mathrm{e}}} \|\bar{\boldsymbol{\rho}}(\boldsymbol{\rho}) - \bar{\boldsymbol{\rho}}^{\star}\|_2^2 \tag{9}$$

where the solution $\boldsymbol{\rho}^{\star}$ serves as a corrected input dose in order to create the desired output pattern $\bar{\boldsymbol{\rho}}^{\star}$. With respect to the unit box constraints, it should be noted that the design variables $\boldsymbol{\rho}$ can be scaled to the interval $[0; 1]$ by division by the maximum allowed dose. The threshold η in the projection function is then equal to the ratio of the clearing dose and the maximum dose. The optimization problem can be solved with the method of moving asymptotes (MMA)

(Svanberg 1987) or, since the problem only has box constraints, a projected steepest descent method. The sensitivities of the objective function are determined as follows:

$$\frac{\partial f_{\text{pec}}}{\partial \boldsymbol{\rho}} = \frac{\partial f_{\text{pec}}}{\partial \bar{\boldsymbol{\rho}}} \frac{\partial \bar{\boldsymbol{\rho}}}{\partial \tilde{\boldsymbol{\rho}}} \frac{\partial \tilde{\boldsymbol{\rho}}}{\partial \boldsymbol{\rho}} \tag{10}$$

$$= \frac{2}{n_{\text{e}}} (\bar{\boldsymbol{\rho}} - \bar{\boldsymbol{\rho}}^{\star})^{\text{T}} \frac{\partial \bar{\boldsymbol{\rho}}}{\partial \tilde{\boldsymbol{\rho}}} \frac{\partial \tilde{\boldsymbol{\rho}}}{\partial \boldsymbol{\rho}} \tag{11}$$

where the Jacobians $\frac{\partial \bar{\boldsymbol{\rho}}}{\partial \tilde{\boldsymbol{\rho}}}$ and $\frac{\partial \tilde{\boldsymbol{\rho}}}{\partial \boldsymbol{\rho}}$ follow from differentiation of the projection function (8) and the density filter (7).

The application of topology optimization for PEC is illustrated for a classical example (Haslam and McDonald 1986). The dimensions of the desired written pattern are shown in Fig. 6. The parameters of the PSF are $\alpha_{\text{f}} = 0.13\ \mu\text{m}$, $\alpha_{\text{b}} = 1\ \mu\text{m}$ and $\tau = 1.15$. For simplicity the maximum dose is set equal to twice the clearing dose such that the projection threshold is $\eta = 0.5$. A fixed steepness parameter $\beta = 64$ is used during the optimization. The domain is discretized into 200×200 pixels.

The top row of Fig. 7 shows what would happen if the desired pattern $\bar{\boldsymbol{\rho}}^{\star}$ is used as input dose for the EBL system. It can seen that the energy leakage reduces the size of the small square object and causes the manufactured pattern $\bar{\boldsymbol{\rho}}(\bar{\boldsymbol{\rho}}^{\star})$ to contain rounded corners. Furthermore, the thin gap between the two rectangles is closed due to the proximity effect.

Next, the optimization problem (9) is solved in order to improve the input $\boldsymbol{\rho}$. The bottom row of Fig. 7 shows the situation where the solution $\boldsymbol{\rho}^{\star}$ is used as input. A number of corrections can be seen in the modified input $\boldsymbol{\rho}^{\star}$: serifs are added to the corners of objects in order to correct for the rounded corners and the gap between the two rectangles is slightly enlarged to compensate for the proximity effect. As a result, the pattern fidelity of the fabricated design $\bar{\boldsymbol{\rho}}(\boldsymbol{\rho}^{\star})$ is strongly improved.

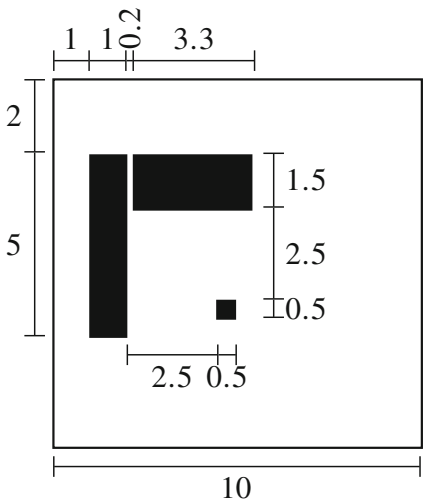

Fig. 6 Target written pattern $\bar{\boldsymbol{\rho}}^{\star}$. Dimensions are in μm

5 Dose regularization

Due to the combined smoothing and projection operation in the filter, the inverse problem of finding the correct dose pattern $\boldsymbol{\rho}$ for a given final design $\bar{\boldsymbol{\rho}}$ is an ill-posed problem. The solution of the problem is non-unique since a single design $\bar{\boldsymbol{\rho}}$ can be generated from different inputs $\boldsymbol{\rho}$. For this reason, the inputs found by proximity effect correction will often be contaminated by noise in the void and material phases.

Similar phenomena occur when a projection filter is applied in topology optimization. This issue has not yet received much attention in the topology optimization literature due to the irrelevant nature of the design field $\boldsymbol{\rho}$, but in a lithographic setting, a complex dose $\boldsymbol{\rho}$ increases the writing time of the lithography system and spending energy on reproducing unnecessary features should be avoided.

The image of the input $\boldsymbol{\rho}$ can be improved by introducing regularization[2] with respect to $\boldsymbol{\rho}$ in the optimization problem. The regularization term $f_{\text{reg}}(\boldsymbol{\rho})$ is added as a penalty term to the objective function:

$$\tilde{f}_0(\boldsymbol{\rho}) = f_0(\boldsymbol{\rho}) + \lambda f_{\text{reg}}(\boldsymbol{\rho}) \tag{12}$$

where λ is a weight parameter. A number of regularization terms f_{reg} are investigated for this purpose.

An important drawback of EBL is the low throughput caused by the relatively high writing time required to expose the resist. Since the writing time is determined by the dose, it is relevant to penalize the total dose in order to decrease the production time:

$$V(\boldsymbol{\rho}) = \frac{1}{V_{\Omega}} \sum_{e=1}^{n_{\text{e}}} v_e \rho_e \tag{13}$$

Where $V_{\Omega} = \sum_{e}^{n_{\text{e}}} v_e$ is the volume of the design domain. The volume fraction $V(\boldsymbol{\rho})$ represents an L^1-regularization.

In some EBL systems, the dose is limited to one constant value (Lee et al. 1991) which means the design variables should resemble a binary input. Extending the applicability of the proposed approach for mask design in optical lithography (see Section 8) requires the input to be binary in order to mimic the application of a mask to expose certain parts of the design domain. A binary design can be enforced in the

[2]It should be pointed out that the term regularization is often used in lithography to describe techniques for cleaning the dose pattern which differs from topology optimization where regularization is used for ensuring existence of the solution.

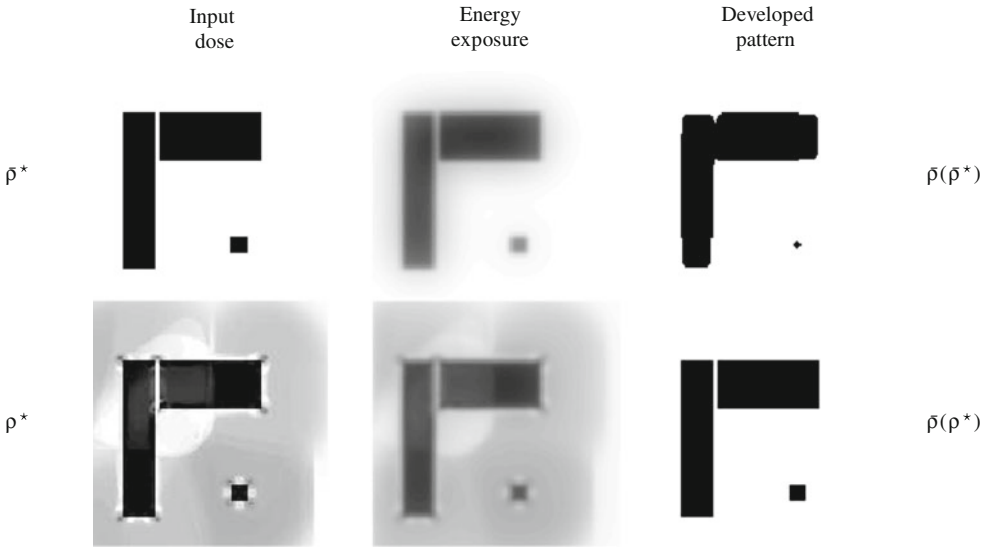

Fig. 7 Proximity effect correction of pattern $\bar{\boldsymbol{\rho}}^\star$. The situation where an uncorrected input is used, is illustrated in the *top row*. The corrected input is shown in the *bottom row*

optimization by penalizing the mean non-discreteness of the optimization variables (Sigmund 2007):

$$M_{\mathrm{nd}}(\boldsymbol{\rho}) = \frac{4}{n_{\mathrm{e}}} \sum_{e=1}^{n_{\mathrm{e}}} (\rho_e(1-\rho_e)) \tag{14}$$

It should be noted that M_{nd} forms a non-convex function as opposed to the other penalty terms presented here which are all convex functions.

The third dose cleaning technique avoids excessively complicated inputs. The complexity can be measured by the total variation (Petersson 1999):

$$TV(\boldsymbol{\rho}) = \frac{1}{n_{\mathrm{e}}} \sum_{e=1}^{\tilde{n}_{\mathrm{e}}} \sqrt{(\mathsf{D}_x\boldsymbol{\rho})_e^2 + (\mathsf{D}_y\boldsymbol{\rho})_e^2} \tag{15}$$

where D_x and D_y are the finite difference tensors for the discretization of the domain with zero-padded edges. Alternatively, the complexity of only the parts which differ from the physical design can be penalized: $f_{\mathrm{reg}}(\boldsymbol{\rho}) = TV(\boldsymbol{\rho}-\bar{\boldsymbol{\rho}}^\star)$ (Poonawala and Milanfar 2007).

Figure 8 shows proximity effect corrected designs obtained with the different penalty terms. The weight parameter in (12) is fixed equal to $\lambda = 0.2$ in all cases. Although the solutions $\boldsymbol{\rho}^\star$ obtained with the different regularization terms (Fig. 8 top row) show significant differences, the resulting patterns $\bar{\boldsymbol{\rho}}(\boldsymbol{\rho}^\star)$ (Fig. 8 bottom row) correspond very well to the target pattern $\bar{\boldsymbol{\rho}}^\star$. The volume penalty $V(\boldsymbol{\rho})$ strongly reduces the total dose: the volume fraction of the solution with penalization (Fig. 8b) is only $V(\boldsymbol{\rho}^\star) = 9\ \%$ compared to $V(\boldsymbol{\rho}^\star) = 20\ \%$ for the original solution (Fig. 8a) which results in a more than two times faster production process.

The penalization form given by (14) results in crisp black and white design. The pattern volume is larger compared to the volume penalization case, however due to the discreteness of the design, the pattern is applicable not only in EBL but also for mask design in optical lithography.

Total variation terms (Fig. 8d–e) effectively reduce the fluctuations in the solution. It can be seen that the term $TV(\boldsymbol{\rho})$ also reduces the contrast in the solution $\boldsymbol{\rho}^\star$ at the transitions zones between black and white in the pattern (Fig. 8d) which could have a negative influence on the robustness of the design (see Section 6). On the other hand, the edges in the solution $\boldsymbol{\rho}^\star$ with the difference term $TV(\boldsymbol{\rho}-\bar{\boldsymbol{\rho}}^\star)$ (Fig. 8e) remain crisp.

6 Imperfections and robustness

The previous sections demonstrate that electron beam lithography and proximity effects can be modeled with projection filtering in topology optimization if the design variables $\boldsymbol{\rho}$ are identified as the input dose $D(\mathbf{x})$ in electron beam lithography. This observation enables us to perform numerical proximity effect correction of the input dose $\boldsymbol{\rho}$ for a given pattern $\bar{\boldsymbol{\rho}}$.

However, the robustness of the solution obtained remains to be investigated: in reality, imperfections in the lithographic process have a considerable influence on the resulting pattern (Dobisz and Marrian 1997). The development phase, for example, does not behave as a perfect threshold, but is instead governed by complex reaction-diffusion processes. During the exposure, variation in the dose, charging of the resist and misalignment of the setup are known to cause uncertainties in the exposure (Dobisz et al. 2007). Furthermore, closely spaced objects are more sensitive with respect to variations in the system due to the smaller

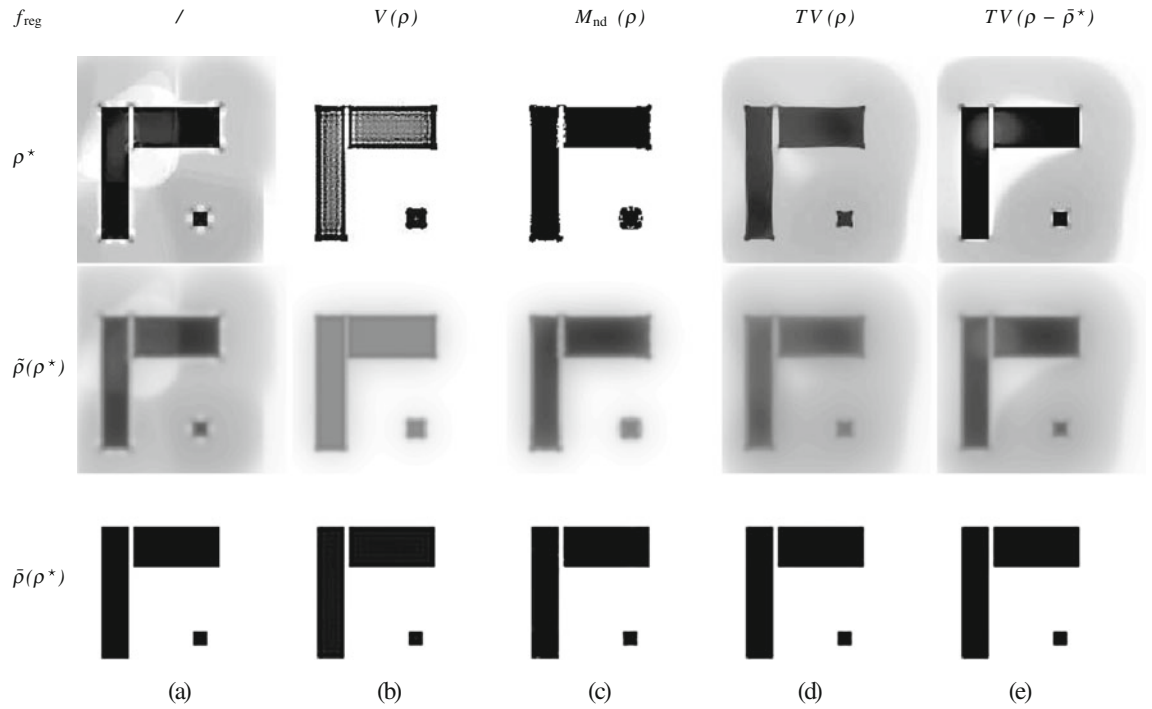

Fig. 8 Proximity corrected inputs with different regularization terms

intermediate energy contrast caused by the proximity effect.

The effect of uncertainties in the EBL process can be modeled by varying the Heaviside projection threshold η (Sigmund 2009; Wang et al. 2011b). Variations of the Heaviside projection threshold η in the topology optimization formulation correspond to variations of the clearing energy E_{cl} in the EBL procedure, resulting in a dilation or an erosion effect. In the following, the nominal projection threshold is denoted as η_{i}. This projection threshold results in the nominal (or intermediate) pattern $\bar{\boldsymbol{\rho}}^{\text{i}} = H_{\text{c}}(\tilde{\boldsymbol{\rho}}; \eta_{\text{i}}, \beta)$. A lower projection threshold $\eta_{\text{d}} < \eta_{\text{i}}$ results in a dilated pattern $\bar{\boldsymbol{\rho}}^{\text{d}} = H_{\text{c}}(\tilde{\boldsymbol{\rho}}; \eta_{\text{d}}, \beta)$, while a higher projection threshold $\eta_{\text{e}} > \eta_{\text{i}}$ results in an eroded pattern $\bar{\boldsymbol{\rho}}^{\text{e}} = H_{\text{c}}(\tilde{\boldsymbol{\rho}}; \eta_{\text{e}}, \beta)$.

Figure 9 shows the patterns obtained for the input dose in Fig. 3a with three different projection thresholds $\eta_{\text{d}} < \eta_{\text{i}} < \eta_{\text{e}}$. The dilation/erosion effect is clearly visible. Moreover, we can observe an increased sensitivity of closely spaced objects with respect to imperfections: while the pattern errors in the bars on the left side of the grid are relatively small, the shape of the bars on the right side changes strongly between the dilated and eroded design. We therefore conclude that a Heaviside projection filter with a variable threshold is capable of reproducing the proximity effect. This is explained as follows: when a variable threshold is applied, the geometric variations in the design $\bar{\boldsymbol{\rho}}$ coincide with the region where the exposure $\tilde{\boldsymbol{\rho}} \in [\eta_{\text{d}}; \eta_{\text{e}}]$. The size of this region $\Delta\bar{\boldsymbol{\rho}}$ is clearly minimized by maximizing the slope in $\tilde{\boldsymbol{\rho}}$. Figure 10 illustrates this by comparing the geometric variations $\Delta\bar{\boldsymbol{\rho}}$ for two different profiles $\tilde{\boldsymbol{\rho}}$. When the distance between two objects in

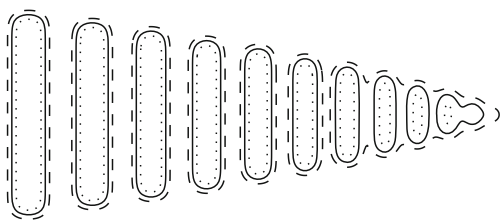

Fig. 9 Proximity effect sensitivity modeled by the robust projection filter. *Dashed line*: $\bar{\boldsymbol{\rho}}^{\text{d}}$, *full line*: $\bar{\boldsymbol{\rho}}^{\text{i}}$, *dotted line*: $\bar{\boldsymbol{\rho}}^{\text{e}}$

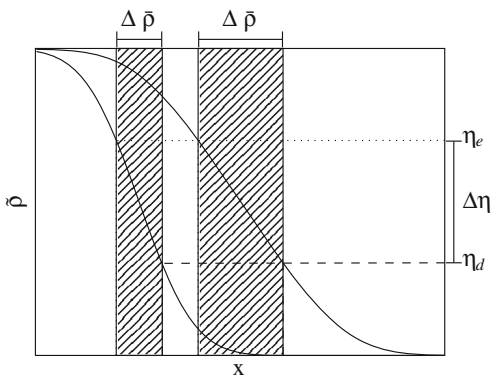

Fig. 10 Slope dependence of imperfections modeled by means of a variable Heaviside projection threshold

the input dose $\boldsymbol{\rho}$ decreases, the slope in the energy exposure $\tilde{\boldsymbol{\rho}}$ reduces due to an increase in mutual energy exchange. As a consequence, the geometric variations due to a variable threshold increase and the objects become more sensitive to errors in the EBL process.

Next, the input dose $\boldsymbol{\rho}^\star$ identified in Section 4 is reconsidered. Figure 11 shows the dilated pattern $\bar{\boldsymbol{\rho}}^{\mathrm{d}} = H_{\mathrm{c}}(\tilde{\boldsymbol{\rho}}; \eta_{\mathrm{d}}, \beta)$, the intermediate pattern $\bar{\boldsymbol{\rho}}^{\mathrm{i}} = H_{\mathrm{c}}(\tilde{\boldsymbol{\rho}}; \eta_{\mathrm{i}}, \beta)$, and the eroded pattern $\bar{\boldsymbol{\rho}}^{\mathrm{e}} = H_{\mathrm{c}}(\tilde{\boldsymbol{\rho}}; \eta_{\mathrm{e}}, \beta)$, obtained with the projection thresholds $\{\eta_{\mathrm{d}}; \eta_{\mathrm{i}}; \eta_{\mathrm{e}}\} = \{0.4; 0.5; 06\}$. It should be noted that the interval is based on the authors' experience with etching processes and chosen for illustrative reasons only. In reality, the interval should be calibrated to the actual production process. The design $\bar{\boldsymbol{\rho}}^{\mathrm{i}}$ obtained with the intermediate value η_{i} is obviously identical to the design obtained in Section 4, and very similar to the target pattern $\bar{\boldsymbol{\rho}}$. This does not hold for the dilated and eroded designs $\bar{\boldsymbol{\rho}}^{\mathrm{d}}$ and $\bar{\boldsymbol{\rho}}^{\mathrm{e}}$, however. The variation of the projection threshold leads to a considerable under- or over-etching effect, serifed or rounded corners, and closing or widening of the gap between the rectangles. These phenomena are quite similar to the original proximity effect – we therefore have to conclude that the input dose $\boldsymbol{\rho}^\star$ found in Section 4 is not robust with respect to uncertainties in the EBL process.

High contrast between the material and void phase in the dose pattern can contribute to steep transitions in the exposure which reduces the extent of the geometric imperfections. In this respect, regularization of the dose also indirectly affects the robustness of the optimized design with respect to manufacturing errors. Comparison of the dose patterns and energy exposures in Fig. 8 gives a qualitative overview of the effect of the different regularization terms on the expected geometric imperfections. The non-discreteness function (14) clearly tends to maximize the contrast in the dose which results in steep gradients of the exposure in the transition zones. The total variation (15) on the other hand penalizes variations and therefore reduces the contrast in the dose. It can be seen that this drawback is avoided to some extent by applying the difference term $TV(\boldsymbol{\rho} - \bar{\boldsymbol{\rho}}^\star)$ which results in sharper edges in the dose. Nevertheless, improvements such as a high contrast in itself do not suffice to ensure robustness of the design.

In order to obtain a more robust solution, the effect of a varying projection threshold is taken into account in the optimization. Projection threshold variability can be modeled by means of a worst case approach (Wang et al. 2011b) or a probabilistic approach (Lazarov et al. 2011; Schevenels et al. 2011). A worst case approach is followed here; the robust optimization problem is formulated as a minimax problem:

$$\boldsymbol{\rho}^\star = \arg\min_{0 \le \boldsymbol{\rho} \le 1} \max \left\{ f_{\mathrm{pec}}(\bar{\boldsymbol{\rho}}^{\mathrm{d}}),\ f_{\mathrm{pec}}(\bar{\boldsymbol{\rho}}^{\mathrm{i}}),\ f_{\mathrm{pec}}(\bar{\boldsymbol{\rho}}^{\mathrm{e}}) \right\} \tag{16}$$

Figure 13a shows the robust input dose $\boldsymbol{\rho}^\star$ thus obtained, Fig. 13b shows the effect of the PSF, and Fig. 13c–e show the final pattern in the case of maximum dilation, the intermediate case, and the case of maximum erosion. The corresponding performance is illustrated in Fig. 12 where the pattern fidelity f_{pec} is shown as a function of the projection threshold η. Compared to the pattern obtained with the original input dose (Fig. 11), the pattern obtained with the robust dose is clearly less sensitive to projection threshold variations, and therefore also to the uncertainties in the EBL process. On the other hand, the nominal design $\bar{\boldsymbol{\rho}}^{\mathrm{i}}$ obtained with an intermediate projection threshold η_{i} is clearly different from the target pattern $\bar{\boldsymbol{\rho}}^\star$. This trade-off effect between nominal performance and (in)sensitivity to uncertainties is a typical property of robust optimization problems.

Finding a dose that is completely insensitive with respect to imperfections in the EBL process is physically impossible: due to the spreading of energy, the slope of the exposure $\tilde{\boldsymbol{\rho}}$ is always finite, and this will always result in a dilation or erosion effect when the clearing energy E_{cl} (or the projection threshold η) varies. In the example shown in Fig. 13, variations of the projection threshold even lead to changes in the topology of the pattern: the gap between the two

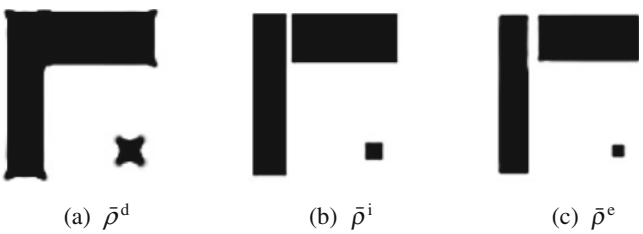

Fig. 11 Influence of uncertainties in the EBL process: pattern obtained with the nominal input dose $\boldsymbol{\rho}^\star$ in combination with different projection thresholds; (**a**) $\eta_{\mathrm{d}} = 0.4$, (**b**) $\eta_{\mathrm{i}} = 0.5$, and (**c**) $\eta_{\mathrm{e}} = 0.6$

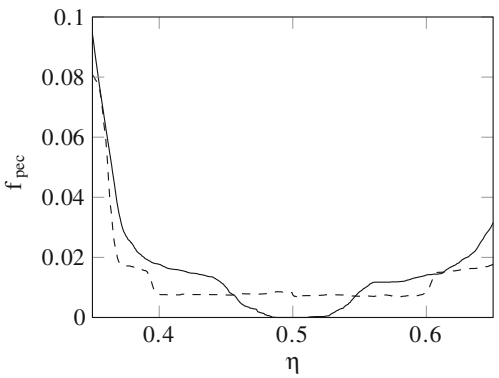

Fig. 12 Pattern fidelity f_{pec} as a function of the projection threshold η for the nominal design (*solid line*) and the robust design (*dashed line*)

(a) $\rho^\star$ (b) $\tilde{\rho}$ (c) $\bar{\rho}^{\mathrm{d}}$ (d) $\bar{\rho}^{\mathrm{i}}$ (e) $\bar{\rho}^{\mathrm{e}}$

Fig. 13 **a** Robust dose $\boldsymbol{\rho}^\star$ obtained by incorporating geometric imperfections in the proximity effect correction, (**b**) intermediate variables $\tilde{\boldsymbol{\rho}}$, and (**c**–**e**) resulting patterns for different projection thresholds; (**c**) $\eta_{\mathrm{d}} = 0.4$, (**d**) $\eta_{\mathrm{i}} = 0.5$, and (**e**) $\eta_{\mathrm{e}} = 0.6$

large rectangles is closed unless the projection threshold η is high. This effect is not surprising: as we followed a least squares approach, we did not penalize changes of topology in the formulation of the robust optimization problem (16). Whether a change of topology is important depends on the type of the problem: for some applications, the performance of a design will be highly dependent on the topology, while for others, it may be rather insensitive. In order to properly take into account the impact of topological changes on the performance, the following section addresses a case where the performance of the design is optimized, and the design itself becomes a variable in the optimization procedure.

7 Design optimization

In this section the focus is on the optimal design of a compliant inverter, which is a classical benchmark problem in the domain of topology optimization (Sigmund 1997). Due to the similarities of the EBL process and the projection method for topology optimization, the optimized design variables $\boldsymbol{\rho}^\star$ can immediately be interpreted as an EBL input dose, provided that we choose the appropriate density filter kernel and Heaviside projection threshold. Several regularization schemes are investigated and their impact on the optimized input dose and the corresponding pattern is assessed.

The design domain and boundary conditions of the problem are shown in Fig. 14. The goal of the inverter is to

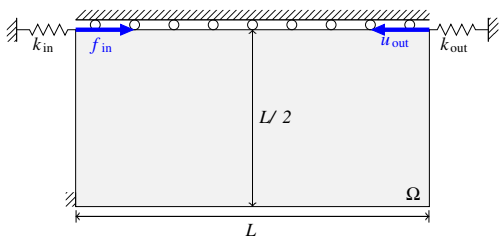

Fig. 14 Design domain and boundary conditions for the compliant inverter problem

maximize the output displacement u_{out} when the input force f_{in} is applied to the mechanism. The volume fraction of the nominal design $V(\bar{\boldsymbol{\rho}}^{\mathrm{i}}(\boldsymbol{\rho}))$ is limited to $V_{\max} = 0.3$. The design domain with length $L = 300\ \mu$m and thickness $t = 1\ \mu$m is discretized into 200×100 square finite elements. The displacements $u(\bar{\boldsymbol{\rho}})$ for a physical design $\bar{\boldsymbol{\rho}}$ follow from the finite element analysis:

$$\mathsf{K}(\bar{\boldsymbol{\rho}})\mathbf{u}(\bar{\boldsymbol{\rho}}) = \mathbf{f} \tag{17}$$

where $\mathbf{f}$ is the external force vector which contains $f_{\mathrm{in}} = 1$ mN at the correct degree of freedom and K is the global stiffness matrix. The SIMP interpolation (6) with $E_0 = 1$ GPa and $E_{\min} = 10^{-9}E_0$ and a Poisson's ratio $\nu = 0.3$ are used as material properties in the evaluation of the element stiffness matrices $\mathsf{K}_e = E_e\mathsf{K}_0$. The input and output springs stiffness coefficients are $k_{\mathrm{in}} = 1\ \mathrm{mN}/\mu\mathrm{m}$ and $k_{\mathrm{out}} = 0.005\ \mathrm{mN}/\mu\mathrm{m}$, respectively. In a minimization problem, the objective function f_0 is expressed as:

$$f_0(\bar{\boldsymbol{\rho}}) = -u_{\mathrm{out}}(\bar{\boldsymbol{\rho}}) = \mathbf{b}^{\mathrm{T}}\mathbf{u}(\bar{\boldsymbol{\rho}}) \tag{18}$$

where the vector $\mathbf{b}$ selects the output displacement u_{out} from the displacement vector $\mathbf{u}$. The double Gaussian PSF (2) is applied as the density filter kernel with parameters $\alpha_{\mathrm{f}} = 3\ \mu$m, $\alpha_{\mathrm{b}} = 20\ \mu$m and $\tau = 0.5$. The uncertainties in the production process are modeled by the robust projection filter with $\{\eta_{\mathrm{d}}; \eta_{\mathrm{i}}; \eta_{\mathrm{e}}\} = \{0.4; 0.5; 06\}$. In this case, the inverter design problem is formulated as a minimax problem:

$$\begin{aligned} \min_{\boldsymbol{\rho}} \quad & f_{\mathrm{r}}(\boldsymbol{\rho}) = \max\left\{ f_0(\bar{\boldsymbol{\rho}}^{\mathrm{d}}(\boldsymbol{\rho})),\ f_0(\bar{\boldsymbol{\rho}}^{\mathrm{i}}(\boldsymbol{\rho})),\ f_0(\bar{\boldsymbol{\rho}}^{\mathrm{e}}(\boldsymbol{\rho}))\right\} \\ \text{s.t.} \quad & V(\bar{\boldsymbol{\rho}}^{\mathrm{d}}(\boldsymbol{\rho})) - V_{\max}^{\mathrm{d}} \le 0 \\ & \mathbf{0} \le \boldsymbol{\rho} \le \mathbf{1} \end{aligned} \tag{19}$$

The volume fraction of the dilated design $\bar{\boldsymbol{\rho}}^{\mathrm{d}}$ is constrained as discussed by (Wang et al. 2011b): the maximum volume fraction $V_{\max}^{\mathrm{d}}$ is adapted during the optimization such that the volume fraction of the nominal design $V(\bar{\boldsymbol{\rho}}^{\mathrm{i}})$ remains

below $V_{\max}$. The sensitivities with respect to the physical design $\bar{\boldsymbol{\rho}}$ are determined by means of the adjoint method:

$$\frac{\partial f_0}{\partial \bar{\boldsymbol{\rho}}} = -\mathbf{v}^{\mathrm{T}} \frac{\partial \mathsf{K}}{\partial \bar{\boldsymbol{\rho}}} \mathbf{u} \tag{20}$$

where the adjoint variable $\mathbf{v}$ solves the linear system $\mathsf{K}\mathbf{v} = \mathbf{b}$. The sensitivities with respect to $\boldsymbol{\rho}$ are again found as in (10) by applying the chain rule of differentiation twice. The optimization problem is solved by means of the method of moving asymptotes (Svanberg 1987).

The design obtained for problem (19) is shown in the top row of Fig. 15. Although the physical densities $\bar{\boldsymbol{\rho}}^{\mathrm{i}}$ form a clean structure, the design variables $\boldsymbol{\rho}$ (i.e. the dosage) contain numerous irregularities which should be avoided as input for a lithography system. Therefore, regularization is introduced to the robust objective function in optimization problem (19):

$$\tilde{f}_{\mathrm{r}}(\boldsymbol{\rho}) = f_{\mathrm{r}}(\boldsymbol{\rho}) + \lambda f_{\mathrm{reg}}(\boldsymbol{\rho}) \tag{21}$$

The penalty terms are activated once the projection function (8) has become sufficiently steep (e.g. $\beta \geq 8$) by switching the weight parameter λ from zero to a small positive number. The following results were obtained with a fixed value $\lambda = 0.2$ for all regularization terms. The designs obtained in this way are shown in Fig. 15 and their properties are summarized in Table 1. From these results, it can be seen that the physical designs $\bar{\boldsymbol{\rho}}^{\mathrm{i}}$ for the different situations are almost identical in both topology and performance $f_0(\bar{\boldsymbol{\rho}}^{\mathrm{i}})$. The inputs $\boldsymbol{\rho}$, on the other hand, differ quite strongly. This already indicates that the topology optimization of the actual physical design $\bar{\boldsymbol{\rho}}$ is relatively insensitive with respect to regularization of the optimization variables $\boldsymbol{\rho}$. Including an L^1-regularization such as the total dose $V(\boldsymbol{\rho})$ typically leads to a sparser solution for $\boldsymbol{\rho}$. The total dose is strongly reduced (cf. Table 1), but is configured such that the intermediate design $\tilde{\boldsymbol{\rho}}$ remains above the highest threshold η_{e} where needed to keep the physical design unaltered. As expected, inclusion of the mean non-discreteness penalty $M_{\mathrm{nd}}(\boldsymbol{\rho})$ delivers a clean $0-1$ design which can be useful for a constant dose EBL system or mask design in optical lithography. It can be seen that the total variation penalties $TV(\boldsymbol{\rho})$ and $TV(\boldsymbol{\rho} - \bar{\boldsymbol{\rho}}^{\mathrm{i}})$ are useful for removing numerical noise in the void and material phases and reduce the overall complexity of the dosage pattern.

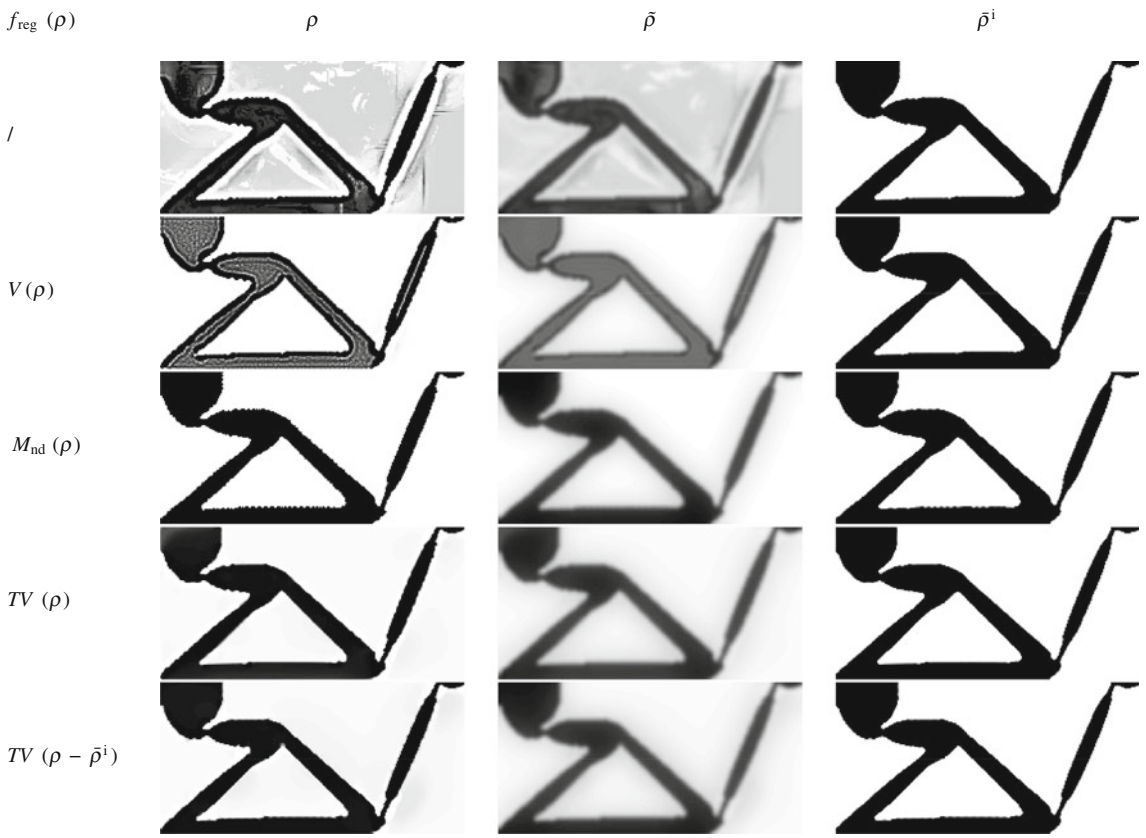

Fig. 15 Designs for the compliant inverter with different regularization terms

Table 1 Optimization results for the compliant inverter obtained with different regularization terms

$f_{\text{reg}}(\boldsymbol{\rho})$	$f_0(\bar{\boldsymbol{\rho}}^{\text{i}})$ [μm]	$V(\boldsymbol{\rho})$ [%]	$M_{\text{nd}}(\boldsymbol{\rho})$ [%]	$TV(\boldsymbol{\rho})$ [%]	$TV(\boldsymbol{\rho}-\bar{\boldsymbol{\rho}}^{\text{i}})$ [%]
/	−2.40	37	32	6.4	4.0
$V(\boldsymbol{\rho})$	−2.40	24	12	8.2	7.3
$M_{\text{nd}}(\boldsymbol{\rho})$	−2.40	30	1	4.8	2.7
$TV(\boldsymbol{\rho})$	−2.39	30	15	4.1	2.4
$TV(\boldsymbol{\rho}-\bar{\boldsymbol{\rho}}^{\text{i}})$	−2.40	30	11	4.4	1.0

8 Optical lithography

The projection filter in topology optimization can be adopted to model optical lithography as well. The procedure of optical lithography is similar to EBL and also consists of an exposure and development phase (Levinson and Arnold 1997). The photo-sensitive resist is exposed to a light source instead of an electron beam. The light is guided through a mask in order to locally expose the resist. Therefore, the mask geometry $M(\mathbf{x})$ serves as the input for the optical lithography system. As opposed to electron beam lithography where the e-beam is directed onto the resist by a deflector, it is important to note that the mask represents a binary valued variable since it can only be used to either block or transmit light.

The molecular changes in the resist and the thresholding during development phase are related to the light intensity $I(\mathbf{x})$ to which the resist is exposed. Proximity effects are also present in optical lithography where diffraction of light in the optical system causes similar blurring effects of the input as electron scattering in EBL (Levinson and Arnold 1997). If a coherent optical system is assumed, the intensity can be approximated by smoothing the mask image $M(\mathbf{x})$ with a complex point spread function $F(\mathbf{x})$ (Poonawala and Milanfar 2007; Jia et al. 2008; Choy et al. 2012):

$$I(\mathbf{x}) = |(F * M)(\mathbf{x})|^2 \tag{22}$$

Notice that the mask and the intensity are related quadratically instead of linearly. In reality, however, the imaging system behaves as a partially coherent optical system which is described by the Hopkins diffraction model (Hopkins 1953; Born et al. 2000). The intensity on the resist $I(\mathbf{x})$ is formulated as a bilinear mapping of the mask pattern $M(\mathbf{x})$:

$$I(\mathbf{x}) = \int \int_{\mathbb{R}^2} \gamma(\mathbf{s}-t) F(\mathbf{x}-\mathbf{s}) M(\mathbf{s}) F^*(\mathbf{x}-t) M(t) \mathrm{d}\mathbf{s}\mathrm{d}t \tag{23}$$

where the complex degree of coherence $\gamma(\mathbf{s}-t)$ describes the interaction of waves originating from points $\mathbf{s}$ and t on the mask. In a coherent system $\gamma(\mathbf{s}-t) = 1$ everywhere and expression (22) is retrieved. From a computational point of view, it is beneficial to approximate a partially coherent system by a truncated Sum Of Coherent Systems (SOCS) (Pati and Kailath 1994; Cobb 1998):

$$I(x) = \sum_{k=1}^{N} \gamma_k \, |(F_k * M)(\mathbf{x})|^2 \tag{24}$$

where γ_k and $F_k(\mathbf{x})$ are eigenvalues and eigenfunctions related to the partially coherent system. In this way, the partially coherent system is replaced by a squared sum of coherent (linear) systems. Compared to a linear EBL system or a coherent optical system, an additional convolution has to be performed for every additional SOCS mode. Similar to the Karhunen-Loeve expansion of a random field, the truncated SOCS representation is optimal in the sense that error after truncation is minimized and the number of modes to be included is usually small $N \approx 5$ (Cobb 1998).

9 Conclusions and future work

The article provides a physical analogy between projection approaches in topology optimization and electron beam lithography production processes. This enables the application of topology optimization for proximity effect correction in electron beam lithography. Several techniques for simplifying dose patterns and decreasing the production time are demonstrated. The uncertainties in the production process are incorporated in the optimization algorithm which results in manufacturable designs whose performance is insensitive with respect to geometric variations. The variable threshold approach serves as a simplified model which encompasses all uncertainties present in the model and production process. The modeling uncertainties could be reduced by incorporating more accurate production models for the development phase; for example, by solving the reaction-diffusion equations governing the etching process numerically. Alternatively, a calibrated surrogate model could be employed in case the computational cost for including the reaction-diffusion process in the optimization would be infeasible. Nevertheless, it should be emphasized that these improved models are not able to reduce the physical variations inherently present in the production process. These physical

uncertainties should still be included in the optimization in order to achieve design robustness. Further improvement taking into account more complex and accurate imperfection models such as deflection of e-beam and misalignment of setup can be introduced by a perturbed filter (Jansen et al. 2013) and are also subject to future works. Another interesting extension is incorporating optical lithography in the optimization as outlined in Section 8.

Acknowledgments The authors would like to thank Lars Hagedorn Frandsen of the DTU Fotonik department for fruitful discussions on the topic. This research was supported by the NextTop project sponsored by the Villum Foundation and the KU Leuven - BOF PFV/10/002 OPTEC - Optimization in Engineering Center.

References

Anderson E, Olynick D, Chao W, Harteneck B, Veklerov E (2001) Influence of sub-100 nm scattering on high-energy electron beam lithography. J Vac Sci Technol B 19(6):2504–2507

Andreassen E, Lazarov BS, Sigmund O (2012) Design of manufacturable 3d extremal elastic microstructure. In review

Bendsøe M (1989) Optimal shape design as a material distribution problem. Struct Multidiscip Optim 1:193–202

Bendsøe M, Sigmund O (2004) Topology optimization: theory methods and applications, 2nd edn. Springer, Berlin

Born M, Wolf E, Bhatia A, Clemmow P, Gabor D, Stokes A, Taylor A, Wayman P, Wilcock W (2000) Principles of optics: electromagnetic theory of propagation. Interference and diffraction of light. Cambridge University Press, Cambridge, UK

Bourdin B (2001) Filters in topology optimization. Int J Numer Methods Eng 50(9):2143–2158

Brunner T, Ferguson R (1996) Approximate models for resist processing effects In: Proceedings SPIE 2726, optical microlithography IX, pp 198–207

Bruns T, Tortorelli D (2001) Topology optimization of non-linear elastic structures and compliant mechanisms. Comput Methods Appl Mech Eng 190(26–27):3443–3459

Chang T (1975) Proximity effect in electron-beam lithography. J Vac Sci Technol 12(6):1271–1275

Chen S, Chen W (2011) A new level-set based approach to shape and topology optimization under geometric uncertainty. Struct Multidiscip Optim 44:1–18

Choy S, Jia N, Tong C, Tang M, Lam E (2012) A robust computational algorithm for inverse photomask synthesis in optical projection lithography. SIAM J Imaging Sci 5(2):625–651

Cobb N (1998) Fast optical and process proximity correction algorithms for integrated circuit manufacturing. PhD thesis, University of California at Berkeley

Dill F, Neureuther A, Tuttle J, Walker E (1975) Modeling projection printing of positive photoresists. Electron Devices, IEEE Transactions on 22(7):456–464

Dobisz E, Marrian C (1997) Control in sub-100 nm lithography in SAL-601. J Vac Sci Technol B 15(6):2327–2331

Dobisz E, Bandić Z, Peckerar M (2007) Electron beam nanolithography. In: Suzuki K, Smith B (eds), Microlithography, CRC Press, chap 15, pp 799–836

Guest J, Prevost J, Belytschko T (2004) Achieving minimum length scale in topology optimization using nodal design variables and projection functions. Int J Numer Methods Eng 61(2):238–254

Harafuji K, Misaka A, Nomura N, Kawamoto M, Yamashita H (1993) A novel hierarchical approach for proximity effect correction in electron beam lithography. Comput-Aided Des Integr Circ Syst, IEEE Trans on 12(10):1508–1514

Haslam ME, McDonald JF (1986) Transform based proximity corrections: Experimental results and comparisons. J Vac Sci Technol B 4(1):168–175

Hopkins H (1953) On the diffraction theory of optical images. Proceedings of the Royal Society of London Series A Math Phys Sci 217(1130):408–432

Jang GW, van Dijk N, van Keulen F (2012) Topology optimization of mems considering etching uncertainties using the level-set method. Int J Numer Methods Eng 92(6):571–588

Jansen M, Lombaert G, Diehl M, Lazarov B, Sigmund O, Schevenels M (2013) Robust topology optimization accounting for misplacement of material. Struct Multidiscip Optim 47:317–333

Jia N, Lam E (2011) Pixelated source mask optimization for process robustness in optical lithography. Opt Express 19(20):19,384–19,398

Jia N, Wong A, Lam E (2008) Robust mask design with defocus variation using inverse synthesis. In: Proceedings SPIE 7140, Lithography Asia 2008. pp 71, 401W–71, 401W–10

Lazarov BS, Schevenels M, Sigmund O (2011) Robust design of large-displacement compliant mechanisms. Mech Sci 2(2):175–182

Lazarov BS, Schevenels M, Sigmund O (2012) Topology optimization considering material and geometric uncertainties using stochastic collocation methods. Struct Multidiscip Optim 46:597–612

Lee SY, Jacob J, Chen CM, McMillan J, MacDonald N (1991) Proximity effect correction in electron-beam lithography: a hierarchical rule-based scheme – PYRAMID. J Vac Sci Technol B 9(6):3048–3053

Levinson H, Arnold W (1997) Optical lithography. In: Rai-Choudhury P (ed) Handbook of microlithography, micromachining, and microfabrication, IEE materials & devices series, vol 1, SPIE optical engineering press, chap 1

Madjarova N (1992) Characteristics of the resist development process in electron beam lithography. Microelectron J 23(5):375–381

McCord M, Rooks M (1997) Electron beam lithography. In: Rai-Choudhury P (ed) Handbook of Microlithography, Micromachining, and Microfabrication, IEE materials & devices series, vol 1, SPIE Optical Engineering Press, chap 2

Owen G, Rissman P (1983) Proximity effect correction for electron beam lithography by equalization of background dose. J Appl Phys 54(6):3573–3581

Pati Y, Kailath T (1994) Phase-shifting masks for microlithography: automated design and mask requirements. J Opt Soc Am A 11(9):2438–2452

Peckerar M, Chang S, Marrian C (1995) Proximity correction algorithms and a co-processor based on regularized optimization. I: Description of the algorithm. J Vac Sci Technol B 13(6):2518–2525

Peckerar M, Sander D, Srivastava A, Foli A, Vishkin U (2007) Electron beam and optical proximity effect reduction for nanolithography: new results. J Vac Sci Technol B 25(6):2288–2294

Petersson J (1999) Some convergence results in perimeter-controlled topology optimization. Comput Methods Appl Mech Eng 171(1–2):123–140

Poonawala A, Milanfar P (2007) Mask design for optical microlithography – An inverse imaging problem. Image Processing. IEEE Transactions on 16(3):774–788

Randall J, Ronse K, Marschner T, Goethals AM, Ercken M (1999) Variable-threshold resist models for lithography simulation. In: Proceedings SPIE 3679, optical microlithography, vol XII, pp 176–182

Schevenels M, Lazarov B, Sigmund O (2011) Robust topology optimization accounting for spatially varying manufacturing errors. Comput Methods Appl Mech Eng 200(49–52):3613–3627

Sigmund O (1997) On the design of compliant mechanisms using topology optimization. Mech Struct Mach 25(4):493–524

Sigmund O (2007) Morphology-based black and white filters for topology optimization. Struct Multidiscip Optim 33(4–5): 401–424

Sigmund O (2009) Manufacturing tolerant topology optimization. Acta Mechanica Sinica 25:227–239

Suzuki K (2007) Electron beam lithography systems. In: Suzuki K, Smith B (eds) Microlithography. CRC Press, chap 6, Boca Raton, pp 329–360

Svanberg K (1987) The method of moving asymptotes – a new method for structural optimization. Int J Numer Methods Eng 24:359–373

Wang F, Jensen J, Sigmund O (2011a) Robust topology optimization of photonic crystal waveguides with tailored dispersion properties. J Opt Soc Am B: Opt Phys 28(3):387–397

Wang F, Lazarov B, Sigmund O (2011b) On projection methods, convergence and robust formulations in topology optimization. Struct Multidiscip Optim 43:767–784

Wüest R, Hunziker C, Robin F, Strasser P, Erni D, Jäckel H (2004) Limitations of proximity-effect correction for electron-beam patterning of photonic crystals. In: Proceedings SPIE 5277, photonics: design, technology, and packaging, pp 186–197

Xu S, Cai Y, Cheng G (2010) Volume preserving nonlinear density filter based on heaviside functions. Struct Multidiscip Optim 41:495–505

Yu JC, Yu P (2010) Impacts of cost functions on inverse lithography patterning. Opt Express 18(22):23,331–23,342

Zhou M, Rozvany G (1991) The COC algorithm, part II: topological, geometrical and generalized shape optimizations. Comput Methods Appl Mech Eng 89(1–3):309–336